JOURNAL OF GEOPHYSICAL RESEARCH, VOL. 100, NO. B11, PAGES 22,155–22,171, NOVEMBER 10, 1995

Dilatancy, compaction, and slip instability of a fluid-infiltrated fault

Paul Segall
Department of Geophysics, Stanford University, Stanford, California

James R. Rice
Department of Earth and Planetary Sciences and Division of Applied Sciences
Harvard University, Cambridge, Massachusetts

Abstract. We analyze the conditions for unstable slip of a fluid infiltrated fault using a rate and state dependent friction model including the effects of dilatancy and pore compaction. We postulate the existence of a steady state drained porosity of the fault gouge which depends on slip velocity as $\phi_{ss} = \phi_0 + \varepsilon \ln(v/v_0)$ over the range considered, where v is sliding velocity and ε and v_0 are constants. Porosity evolves toward steady state over the same distance scale, d_c, as "state." This constitutive model predicts changes in porosity upon step changes in sliding velocity that are consistent with the drained experiments of Marone et al. (1990). For undrained loading, the effect of dilatancy is to increase (strengthen) $\partial\tau_{ss}/\partial \ln v$ by $\mu_{ss}\varepsilon/(\sigma - p)\beta$, where μ_{ss} is steady state friction, σ and p are fault normal stress and pore pressure, and β is a combination of fluid and pore compressibilities. Assuming $\varepsilon \sim 1.7 \times 10^{-4}$ from fitting the Marone et al. data, we find the "dilatancy strengthening" effect to be reasonably consistent with undrained tests conducted by Lockner and Byerlee (1994). Linearized perturbation analysis of a single degree of freedom model in steady sliding shows that unstable slip occurs if the spring stiffness is less than a critical value given by $k_{\text{crit}} = (\sigma - p)(b - a)/d_c - \varepsilon\mu_{ss}F(c^*)/\beta d_c$ where a and b are coefficients in the friction law and $F(c^*)$ is a function of the model hydraulic diffusivity c^* (diffusivity/diffusion length^2). In the limit $c^* \to \infty$ $F(c^*) \to 0$, recovering the drained result of Ruina (1983). In the undrained limit, $c^* \to 0$, $F(c^*) \to 1$, so that for sufficiently large ε slip is always stable to small perturbations. Under undrained conditions $(\sigma - p)$ must exceed $\varepsilon\mu_{ss}/\beta(b - a)$ for instabilities to nucleate, even for arbitrarily reduced stiffness. This places constraints on how high the fault zone pore pressure can be, to rationalize the absence of a heat flow anomaly on the San Andreas fault, and still allow earthquakes to nucleate without concommitant fluid transport. For the dilatancy constitutive laws examined here, numerical simulations do not exhibit large interseismic increases in fault zone pore pressure. The simulations do, however, exhibit a wide range of interesting behavior including: sustained finite amplitude oscillations near steady state and repeating stick slip events in which the stress drop decreases with decreasing diffusivity, a result of dilatancy strengthening. For some parameter values we observe "aftershock" like events that follow the principal stick-slip event. These aftershocks are noteworthy in that they involve rerupture of the surface due to the interaction of the dilatancy and slip weakening effects rather than to interaction with neighboring portions of the fault. This mechanism may explain aftershocks that appear to be located within zones of high mainshock slip, although poor resolution in mainshock slip distributions can not be ruled out.

Introduction

In the past decade there has been a great deal of experimental and theoretical research on the nucleation of earthquake slip. Much of this work has stemmed from laboratory friction experiments which showed that the coefficient of friction depends on the history of past slip as well as current slip rate [*Dieterich*, 1978, 1979]. These results led to the development of so-called rate- and state-dependent friction laws [*Ruina*, 1983]. These constitutive laws provide a reasonable explanation for the continuous transition from static to dynamic friction that must occur in nature. Analyses of elastic

Paper number 95JB02403.
0148-0227/95/95JB-02403$05.00

systems with rate- and state-dependent friction exhibit both unstable and stable slip depending on elastic stiffness, in accordance with laboratory observations [*Dieterich,* 1979; *Ruina,* 1983; *Gu et al.,* 1984]. Furthermore, the dependence of frictional strength on slip history offers some explanation for the restrengthening of faults between earthquakes, so that models employing these constitutive relations lead naturally to repetitive earthquake cycles. For these, and other, reasons, numerous modeling studies have employed rate- and state-dependent friction laws [*Tse and Rice,* 1986; *Dieterich,* 1986, 1987 ; *Stuart,* 1988; *Tullis,* 1988; *Horowitz and Ruina,* 1989; *Dieterich,* 1992; *Rice,* 1993].

A limitation of the aforementioned analyses is that they do not explicitly account for variations in pore fluid pressure within the fault zone accompanying fault slip. It has been suggested by a number of workers that elevated fluid pressures play an important role in reducing frictional heat production and determining the state of stress near major fault zones [*Lachenbruch,* 1980; *Rice,* 1992; *Byerlee,* 1990, 1993]. It is well known that increases in pore pressure can destabilize faults by decreasing the effective normal stress. On the other hand, shear induced dilatancy will increase effective normal stresses and act to stabilize faulting [e.g., *Rice,* 1975; *Rudnicki and Chen,* 1988].

Laboratory experiments at high temperatures and pressures have shown that shear induced pore compaction can lead to high pore pressures and low frictional strengths [*Blanpied et al.,* 1991, 1992]. *Sleep and Blanpied* [1992], building on ideas of *Sibson* [1992] and *Sibson et al.* [1988], presented quantitative models of the earthquake cycle with transiently high pore fluid pressures. During the interseismic period, creep processes cause pore compaction and increased pore fluid pressure within the fault zone. In some models [*Sleep and Blanpied,* 1992, model 3, figure 2] the pore pressure within the fault zone may nearly equal the least principal stress acting on the fault zone. Pore pressures continue to rise until a Coulomb slip condition is reached and a model earthquake occurs. Dilatancy accompanying the rapid slip event causes the pore fluid pressure to drop and the cycle to begin anew.

There are a number of unresolved issues concerning models of this sort. *Sleep and Blanpied* [1992] did not consider an explicit instability condition; model earthquakes were imposed when the Coulomb slip condition was met. It is not clear in these models, therefore, whether an inertially limited slip event would occur or whether the fault would simply creep in a stable manner. There are two factors that tend to favor stable sliding. The first is shear-induced dilatancy, as discussed above. The second is that low effective normal stresses, themselves, limit the magnitude of strength drops and thus promote stable slip.

More recently, *Sleep* [1995] presents numerical calculations which include slip weakening, following from rate- and state-dependent friction, frictional dilatancy, and thermal pressurization due to shear heating [*Sibson,* 1973; *Lachenbruch,* 1980; *Mase and Smith,* 1987]. In these models it is assumed that dilatancy continues during dynamic rupture at a rate which is just sufficient to neutralize fluid expansion and pressure rise due to shear heating. *Rice* [1994] presented crustal scale instability analyses for a model like that of *Rice* [1993] but including pressurization by shear heating in the absence of dilatancy.

In this paper we attempt to unify the two classes of earthquake models discussed above. That is, we accept that stick-slip instabilities occur under fully drained (constant pore pressure) conditions, as they surely do in laboratory experiments. We also recognize that fault zone materials are likely to undergo shear induced dilatancy. Our goal then is to understand the conditions for unstable slip in saturated fault zone materials that exhibit dilatancy and pore compaction. We do not consider shear heating here.

Experimental Results

It is well known in soil mechanics that when subject to shear, loose sands and underconsolidated clays compact while dense sands or overconsolidated clays dilate [*Lambe and Whitman,* 1969]. It has been observed that with ongoing deformation the porosity tends to a single value, sometimes termed a critical porosity, or critical void ratio [*Schofield and Wroth,* 1968]. Similar behavior has been observed for simulated fault gouges by *Morrow and Byerlee* [1989], who noted that the amount of dilation also depends on strain rate.

Marone et al. [1990] conducted velocity-stepping experiments in which the porosity changes were measured under nominally drained conditions. In these experiments, water saturated layers of Ottawa sand were sheared between 45° surfaces in steel cylinders. The steel surfaces were roughened to prevent slip from localizing at the sand-steel interface. Three holes into the gouge layer allowed pore pressures to equilibrate with an external fluid reservoir. In the experiments discussed here the gouge layers were 4.0 mm thick. Experiments were conducted at effective normal stresses of 50 and 150 MPa [see *Marone et al.,* 1990; Figures 4 and 11]. In all of the experiments the gouge undergoes an initial compaction followed by a long-duration dilation. The long-duration dilation may be due to experimental set-up or the way in which the artificial gouge is prepared. In either case, it clearly can not continue indefinitely. To focus on the short-term changes in porosity accompanying changes in sliding velocity, we fit a polynomial to the porosity-displacement records and remove the long-wavelength effects (Figure 1). The residual porosity variations show a systematic response to step changes in velocity.

Step increases in velocity are accompanied by increases in porosity (dilatancy), whereas step decreases in sliding velocity are accompanied by decreases in porosity (compaction). With continued sliding at constant velocity the porosity tends toward a "steady state" porosity, although this is less clear in the 50-MPa experiment. The distance scale over which the porosity evolves toward the new steady state is comparable to

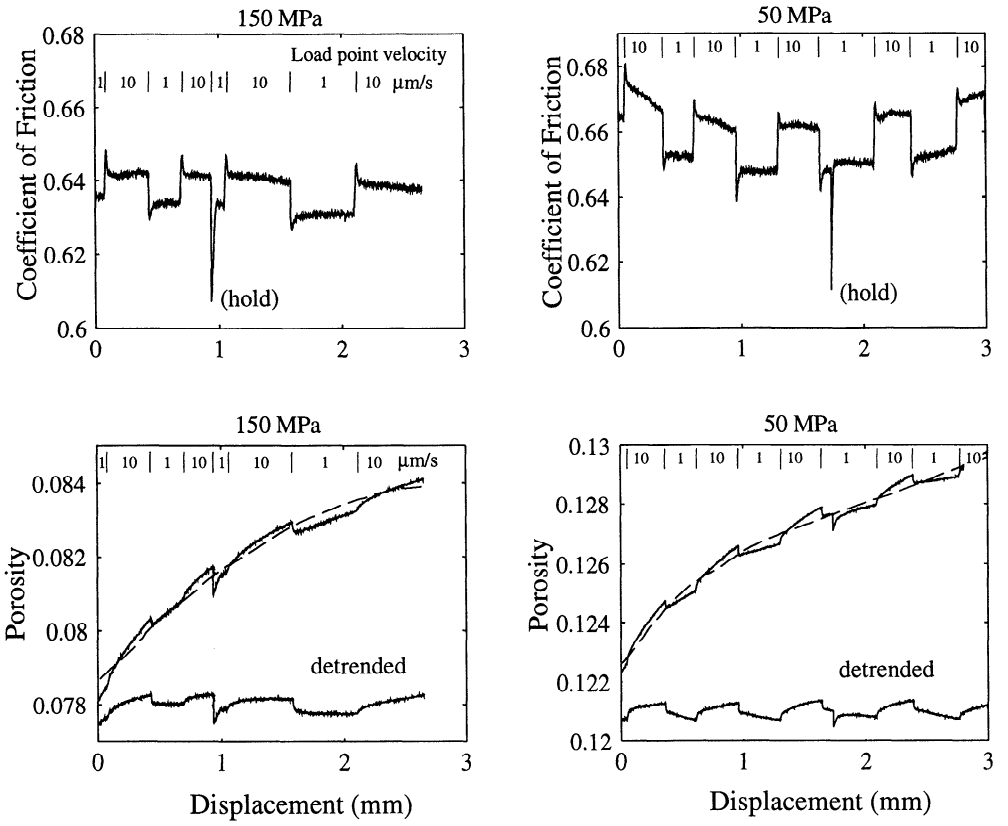

Figure 1. Friction and porosity variations accompanying step changes in sliding velocity, from *Marone et al.* [1990]. (top) Frictional response at (left) 150 MPa and (right) 50 MPa effective normal stress. (bottom) Changes in porosity. Residual porosity variations are shown after removing polynomial fits to the data (dashed lines). The absolute level of detrended porosity is arbitrary.

the distance scale over which the frictional resistance evolves, suggesting that these processes are linked.

Lockner and Byerlee [1994] conducted similar experiments under both nominally drained and undrained conditions. In the drained experiments a single hole allowed fluid communication between the gouge layer and an external reservoir. The drill hole is not present in the undrained experiments. Ottawa sand was placed along a 30° roughened sawcut in Westerly granite cylinders. Gouge thickness was 2.5 mm and the effective normal stress was 50 MPa. The drained tests conducted by *Lockner and Byerlee* [1994] are qualitatively similar to those of *Marone et al.* [1990]. With undrained conditions, however, *Lockner and Byerlee* [1994] find a marked increase in the apparent frictional resistance, which they attribute to decrease in pore pressure within the gouge. We will return to a quantitative analysis of these experiments after introducing the theoretical formulation.

Constitutive Models

Drained Frictional Behavior

We will begin by adopting a simple form of the Dieterich-Ruina friction laws for drained (pore pressure, p, constant) deformation. In this class of constitutive laws the coefficient of friction depends on the instantaneous sliding velocity v and the history of past sliding. The later is incorporated through a state variable θ, that may be interpreted to be the average asperity contact time [*Dieterich*, 1979]. In particular, we take the frictional resistance τ to be given by

$$\tau = (\sigma - p)[\mu_0 + a\ln\frac{v}{v_0} + b\ln\frac{\theta}{\theta_0}] \qquad (1)$$

where σ is normal stress, p is pressure, a and b are constitutive constants, v_0 and θ_0 are normalizing constants, and μ_0 is the nominal friction ($\mu = \mu_0$ for $v = v_0$ and $\theta = \theta_0$).

To complete the description for drained deformation, we must supply an evolution law for the state variable θ. Here we use the "slowness" or "aging" law formalized by *Ruina* [1983] and used extensively by Dieterich,

$$\frac{d\theta}{dt} = 1 - \frac{\theta v}{d_c} \qquad (2)$$

where d_c is the characteristic displacement over which the state variable evolves. Note that θ has units of time and increases linearly when the surfaces are in stationary contact. At steady state, $\theta_{ss} = d_c/v$, the time it

takes the fault to slide a characteristic distance d_c. The evolution law (2) can be written as

$$\frac{d\theta}{dt} = -\frac{v}{d_c}(\theta - \theta_{ss}), \tag{3}$$

which makes clear that, at constant velocity deformation, the state evolves exponentially toward steady state with a characteristic time of d_c/v. An alternate evolution law, called the "slip" law [*Ruina*, 1983], in which $\dot{\theta} \to 0$ as $v \to 0$ as also been widely used. The slip law also reduces to the form (3) for small departures from steady state.

The steady state frictional resistance is given by

$$\tau_{ss} = (\sigma - p)[\mu_0 + (a - b)\ln(\frac{v_{ss}}{v_0})]. \tag{4}$$

For the simple spring slider system (Figure 2) in quasi-static slip, the driving stress rate is given by

$$\frac{d\tau}{dt} = k(v^\infty - v) \tag{5}$$

where k is the spring stiffness, v^∞ is the load point velocity, and v is the slider velocity. It is known that the spring slider system is conditionally stable depending on the spring stiffness, k. When k exceeds a critical value k_{crit} small perturbations are damped, whereas for $k < k_{\text{crit}}$ small perturbations grow in amplitude. For friction laws of the type discussed here, *Ruina* [1983] showed that the critical spring stiffness is given by

$$k_{\text{crit}} = -\frac{1}{d_c}\frac{\partial \tau_{ss}}{\partial \ln v} = (\sigma - p)\frac{(b - a)}{d_c} \tag{6}$$

the latter equality holding for the case in which the steady state friction is given by (4). This expression can be modified for inertial effects, which become important when mv^2 is no longer small compared to $a(\sigma - p)d_c$ [*Rice and Ruina*, 1983]; here m is the mass of the slider per unit area of contact. We are primarily interested here in cases of steady state velocity weakening ($b > a$) since they can lead to instabilities under drained conditions (6), and we wish to see if and how dilatancy and incomplete drainage might stabilize them. Note also that the critical stiffness tends toward zero as the effective stress is reduced. That is, high ambient pore pressure promotes stable sliding as discussed in the introduction.

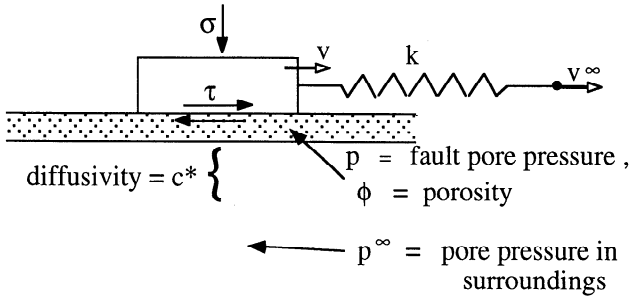

Figure 2. Simple spring slider model.

Governing Equation for Fluid

Continuity of fluid mass in a relatively rigid solid skeleton implies

$$\frac{\partial q_i}{\partial x_i} + \dot{m} = 0, \tag{7}$$

where $\mathbf{q}$ is the fluid mass flux and m is the fluid mass per unit volume of rock. Darcy's law relates fluid flux to pore pressure gradient, via

$$q_i = -\rho_0 \frac{\kappa}{\nu}\frac{\partial p}{\partial x_i} \tag{8}$$

where ρ_0 is the reference fluid density, κ is the permeability, and ν is the pore fluid viscosity. The rate of change of fluid mass can be written as

$$\dot{m} = \rho\dot{\phi} + \phi\dot{\rho} = \rho\dot{\phi} + \phi(\rho\beta_f\dot{p}), \tag{9}$$

where ϕ is porosity and $\beta_f = (1/\rho)(\partial\rho/\partial p)$ is the fluid compressibility. Following *Walder and Nur* [1984], we distinguish between elastic and plastic pore deformation and define an elastic pore compressibility, $\beta_\phi = (1/\phi)(\partial\phi/\partial p)$. Here we neglect full poroelastic coupling and assume that the variation in porosity with respect to pore pressure is for fixed stress normal to the fault zone and fixed strain parallel to the fault zone. Writing the change in porosity as the sum of an elastic and plastic component $\dot{\phi} = \phi\beta_\phi\dot{p} + \dot{\phi}_{\text{plastic}}$ and substituting into (9), we find

$$\dot{m} = \rho[\phi(\beta_f + \beta_\phi)\dot{p} + \dot{\phi}_{\text{plastic}}]. \tag{10}$$

For undrained conditions, $\dot{m} = 0$, (10) gives

$$\dot{p} = -\frac{\dot{\phi}_{\text{plastic}}}{\phi(\beta_f + \beta_\phi)}. \tag{11}$$

For compaction, $\dot{\phi}_{\text{plastic}} < 0$, the pore pressure increases, and for dilation, $\dot{\phi}_{\text{plastic}} > 0$, the pore pressure decreases, as expected.

Substituting (10) and (7) into (8), we find that pore pressure satisfies a diffusion equation, in which the inelastic pore compaction acts as a source term

$$c\nabla^2 p - \frac{\partial p}{\partial t} = \frac{\dot{\phi}_{\text{plastic}}}{\beta} \tag{12a}$$

$$\beta = \phi(\beta_f + \beta_\phi) \tag{12b}$$

$$c = \frac{\kappa}{\nu\beta} \tag{12c}$$

[*Walder and Nur*, 1984]. In the lumped parameter model discussed here, the pore pressure is assumed to follow

$$c^*(p^\infty - p) - \frac{\partial p}{\partial t} = \frac{\dot{\phi}_{\text{plastic}}}{\beta}. \tag{13}$$

Here p refers to the pore pressure within the fault zone, p^∞ refers to the pore pressure in the surroundings, and

the diffusivity is $c^* = c/L^2 = \kappa/\nu\beta L^2$, where L is a characteristic diffusion length. This approximation (13) has previously been used by *Rudnicki and Chen* [1988] in an analysis of laboratory experiments. It may also reasonably apply if the the actively slipping zone is bounded by a cemented border of thickness L which has lower permeability than either the fault zone or the surrounding rock mass. For a homogeneous distribution of properties, L is most naturally associated with the size of the slipping patch; however, a more complete analysis will be necessary to examine this case.

To complete the system, we must have constitutive equations that describe the plastic pore volume change. These are discussed in the next section.

Constitutive Equations for Porosity

Following the critical state concept in soil mechanics, we postulate the existence of a steady state porosity, although here we regard that value as a function of velocity. The experimental data discussed above suggests that at constant slip speed porosity evolves toward steady state over a distance d_c. Thus, by analogy with (3), we consider the simple evolution equation for porosity

$$\dot{\phi} = -\frac{v}{d_c}(\phi - \phi_{ss}), \tag{14}$$

where here, and in what follows, it is implicit that we are referring to inelastic changes in pore volume, i.e., ϕ corresponds to ϕ_{plastic}.

As a starting point, we take the steady state porosity to depend only on velocity. Rapid rates of deformation correspond to greater steady state porosities, while slow rates of deformation correspond to low values of porosity. We postulate the following relation:

$$\phi_{ss} = \phi_0 + \varepsilon \ln\left(\frac{v}{v_0}\right) \tag{15}$$

where ε is a "dilatancy coefficient." Note that the substitution of (15) and (14) into (13) shows that ε and β influence the stress and slip history only through the ratio ε/β.

Equation (15) is incomplete in that it does not limit ϕ to the range $0 \leq \phi \leq 1$. A more general expression for ϕ_{ss} incorporating lower and upper bounds is given by

$$\phi_{ss} = \varepsilon \ln\left[\frac{c_1 v + c_2}{c_3 v + 1}\right], \tag{16}$$

The lower bound on porosity is $\phi_{\min} = \varepsilon \ln(c_2)$, the upper bound is $\phi_{\max} = \varepsilon \ln(c_1/c_3)$. The porosity "saturates" at a velocity of $1/c_3$. At this stage we have not considered a dependence of ε on effective stress, although it seems plausible that ε might decrease with increasing effective stress.

We use (15) and (14) in the present study; however, it should be pointed out that these equations predict no compaction when the fault slip rate vanishes. On the other hand, both bare granite surfaces and simulated granite gouge do show continued porosity reduction in stationary contact (N. Beeler and T.E. Tullis, unpublished manuscript, 1995). An alternate formulation, following *Sleep* [1995], would be to assume that the porosity is function of state, $\phi = \phi(\theta)$, so that the evolution of θ implies an evolution of ϕ. If we employ the "slowness" form of the state evolution equation (2), then ϕ will evolve in stationary contact. In particular, if we adopt

$$\phi = \phi_0 - \varepsilon \ln\left(\frac{v_0 \theta}{d_c}\right) \tag{17}$$

then the steady state porosity is identical to (15), since $\theta_{ss} = d_c/v$. However, from (17) and (2), ϕ decreases with the logarithm of time when $v = 0$, which is qualitatively different from (15) and (14). Although the alternate formulation is distinct, it leads to identical predictions when we study small perturbations from steady state sliding in the section on stability analysis.

Comparison With Experimental Data

In Figure 3 we compare the detrended data from *Marone et al.* [1990] at an effective confining pressure of 150 MPa with the simple constitutive model described

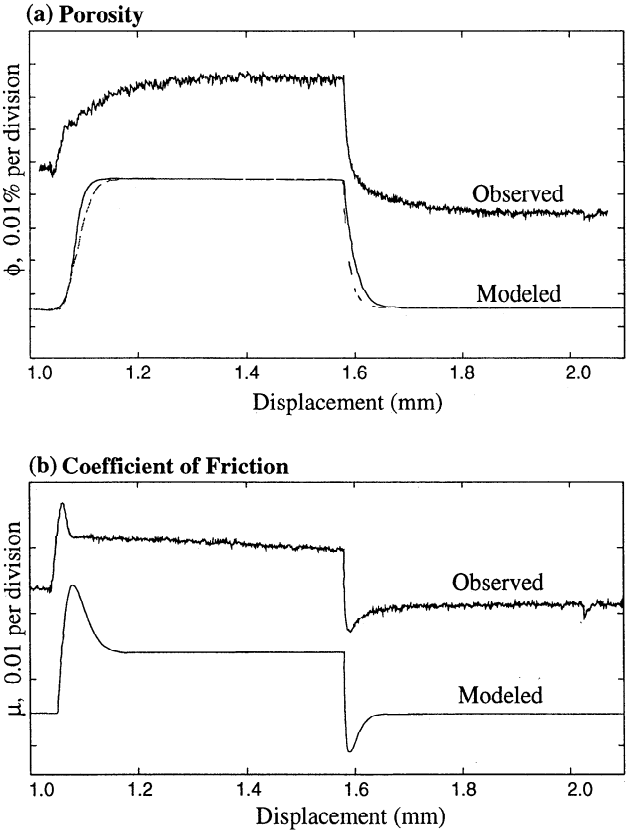

Figure 3. Comparison of observed and predicted response to step increase and decrease in velocity. Initial sliding velocity is 1.0 μ m/s. There is a step up to 10.0 μ m/s and then back to 1.0 μ m/s. (a) Observed and modeled change in porosity. The "observed" porosity is after removal of polynomial as in Figure 1. The solid curve shows the predictions using (14) and (15), while the dashed curve shows the predictions for (17). (b) Observed and modeled frictional response.

above. We model the experiments, using methods described in a later section, including the finite elasticity of the loading system. As discussed above, the porosity evolves over roughly the same distance scale as the friction coefficient, that is there is a single d_c in (2) and (14) or (17). Both constitutive forms, either (14) and (15) or (17), fit the data equally well (Figure 3). By comparing the laboratory data to the simulations (by eye) we infer that the critical displacement d_c is roughly 0.02 mm and that the dilatancy coefficient ε is 1.7×10^{-4}. We also infer $a = 0.010$, $b = 0.006$, and a machine stiffness of the order of 200 MPa/mm. Improved estimates could be obtained with a more formal data fitting scheme [*Reinen and Weeks*, 1993]. Note that the data at 50 MPa do not clearly approach steady state porosity but nevertheless suggests a somewhat larger value of ε. The drained experiments of *Lockner and Byerlee* [1994] are not as easily interpreted but imply a larger dilatancy coefficient.

We would hope to be able to use the results of modeling the drained experiments of *Marone et al.* [1990] to predict the dilatancy strengthening measured by *Lockner and Byerlee* [1994]. Both studies used Ottawa sand to simulate fault gouge; however, other features of the experiments are different, so that we do not expect perfect agreement.

Stability under drained conditions depends on the steady state dependence of friction on the logarithm of velocity (equation (6)). From $\tau = \mu(\sigma - p)$ and the chain rule for differentiation, we may express

$$\left.\frac{d\tau_{ss}}{d\ln v}\right|_m = \left.\frac{d\tau_{ss}}{d\ln v}\right|_p - \mu \left.\frac{dp}{d\ln v}\right|_m , \qquad (18)$$

where the m subscript indicates undrained conditions (constant fluid mass) and the p subscript indicates drained conditions (constant p). Using (11) and (15),

$$\left.\frac{dp}{d\ln v}\right|_m = \left(\frac{dp}{d\phi_{ss}}\right)_m \frac{d\phi_{ss}}{d\ln v} = \frac{-\varepsilon}{\beta}. \qquad (19)$$

This shows that an undrained test will behave like a drained test; however, the steady state velocity dependence will increase (strengthen) by an amount equal to $\mu\varepsilon/\beta$. Dividing both sides by the nominal effective stress allows us to estimate the dilatancy strengthening by

$$\left.\frac{d\mu_{ss}}{d\ln v}\right|_m - \left.\frac{d\mu_{ss}}{d\ln v}\right|_p = \frac{\mu\varepsilon}{(\sigma - p)\phi(\beta_f + \beta_\phi)}. \qquad (20)$$

Lockner and Byerlee [1994] estimate dilatancy strengthening to be in the range 8 to 9 $\times 10^{-3}$ (dimensionless). In their experiments, $\sigma = 100$ MPa, the effective stress is $(\sigma - p) = 50$ MPa, and the nominal friction coefficient is $\mu = 0.7$. The porosity of the gouge is roughly 10% (D. Lockner, personal communication, 1994). The compressibility of water is $\beta_f \sim 4 \times 10^{-4}$ MPa^{-1}, and we may read from Figure 2 of *Zoback and Byerlee* [1976] that the elastic compressibility of Ottawa sand at 50 MPa effective stress is $\beta_\phi \sim 1 \times 10^{-3}$ MPa^{-1}, so that $\beta = \phi(\beta_f + \beta_\phi) \sim 1.4 \times 10^{-4}$. Using the value of ε determined from the *Marone et al.* [1990] experiment, we calculate the strengthening to be 1.6×10^{-2}. This is comparable to, but about a factor of two larger than the values determined by *Lockner and Byerlee* [1994]. On the other hand, ε inferred from Lockner and Byerlee's drained experiments would be consistent with the undrained results only if the pore compressibility is considerably greater.

Stability Analysis

In this section we present a linearized stability analysis of the single degree of freedom system for arbitrary diffusivity. At equilibrium the frictional resistance and the spring force are balanced

$$(\sigma - p)\mu(v, \theta) = k(v^\infty t - u) \qquad (21)$$

where u is displacement, t is time, and the steady state values of the variables are $v_{ss} = v^\infty; \theta_{ss} = d_c/v^\infty; p_{ss} = p^\infty; \tau_{ss} = (\sigma - p^\infty)\mu_{ss}$, as given by (4), and $\phi_{ss} = \varepsilon ln(v^\infty/v_0)$.

Linearizing (21) about steady state, assuming that normal stress is held constant yields

$$(\sigma - p)\left.\frac{\partial\mu}{\partial v}\right|_{ss} \Delta v + (\sigma - p)\left.\frac{\partial\mu}{\partial\theta}\right|_{ss} \Delta\theta - \mu_{ss}\Delta p = -k\Delta u \qquad (22)$$

where the Δ notation signifies departures from steady state. The partial derivatives are evaluated from (1) and considered constants from this point onward in the stability analysis. The state evolution (2) and porosity evolution equation (14) are also linearized, along with the pore pressure diffusion equation (12), as is the relation between displacement and velocity. This yields

$$(\sigma - p)\frac{a}{v^\infty}\Delta\dot{v} = -(\sigma - p)\frac{bv^\infty}{d_c}\Delta\dot{\theta} + \mu_{ss}\Delta\dot{p} - k\Delta v \qquad (23a)$$

$$\Delta\dot{\theta} = -\frac{v^\infty}{d_c}\Delta\theta - \frac{1}{v^\infty}\Delta v \qquad (23b)$$

$$\Delta\dot{\phi} = -\frac{v^\infty}{d_c}\Delta\phi + \frac{\varepsilon}{d_c}\Delta v \qquad (23c)$$

$$\Delta\dot{p} = -\frac{\Delta\dot{\phi}}{\beta} - c^*\Delta p \qquad (23d)$$

$$\Delta\dot{u} = \Delta v \qquad (23e)$$

Equations (23) represent five equations in the five unknowns: $\Delta v, \Delta\theta, \Delta u, \Delta p$, and $\Delta\phi$. Solutions are sought of the form $\Delta p = Pe^{st}$, $\Delta\theta = \Theta e^{st}$, $\Delta v = Ve^{st}, \Delta\phi = \Phi e^{st}$. Substitution of these forms into (23) yields a polynomial equation in s, the roots of which determine the system behavior. If the real part of the roots s_j are negative for all j, the system is linearly stable. If $\Re(s_j) > 0$ for some j, then the system is unstable.

From Appendix A we find that the system is unstable if the spring stiffness is less than a critical value given by

$$k_{crit} = (\sigma - p)\frac{(b-a)}{d_c} - \frac{\varepsilon\mu_{ss}}{\beta d_c}F(c^*) \qquad (24)$$

where the function $F(c^*)$ is given by

$$F(c^*) = \left[\frac{1+\lambda+\gamma}{2} - \sqrt{\frac{(1+\lambda+\gamma)^2}{4} - \gamma}\right] \qquad (25a)$$

$$\lambda = \frac{\beta(\sigma-p)a}{\mu_{ss}\varepsilon}\frac{\xi^2}{\xi+1} \qquad (25b)$$

$$\gamma = \frac{\beta(\sigma-p)(b-a)}{\mu_{ss}\varepsilon}\frac{1}{\xi+1} \qquad (25c)$$

and

$$\xi = \frac{c^* d_c}{v^\infty} \qquad (26)$$

is the ratio of the characteristic time for state evolution to the characteristic time for pore fluid diffusion. In the limit that $c^* \to \infty$, $\gamma \to 0$, and $F(c^*) \to 0$, which recovers the drained result of *Ruina* [1983].

The dependence of critical stiffness on diffusivity $c^* d_c/v^\infty$ is illustrated for a particular set of parameters in Figure 4. With a stiffness slightly in excess of the critical value, $k/k_{\text{crit}} = 1.05$, a small perturbation in velocity causes decaying oscillations in stress (Figure 5, curve A), as well as sliding velocity, porosity, and pore pressure. If the stiffness drops below the critical value, e.g., $k/k_{\text{crit}} = 0.95$, the oscillations increase in amplitude with time (Figure 5, curve B). The linearized analysis does not predict the behavior of the system once the amplitude of the oscillations becomes large. We have conducted numerical solutions of the full set of nonlinear equations (1), (2), (13), (14), (15), and (21), using techniques described in a subsequent section on simulation. We observe that for some range of $k/k_{\text{crit}} < 1.0$ that finite amplitude quasistatic oscillations persist for indefinite time, that is the system of equations exhibits a limit cycle. The transition from a stable point to a limit cycle represents a Hopf bifurcation at $k/k_{\text{crit}} = 1.0$. According to the theory of Hopf bifurcations, the amplitude of the stable oscillations should increase with decreasing k/k_{crit}, as is observed in Figure 5. If k/k_{crit} is sufficiently small, stable limit cycles can not exist and the slip speed becomes unbounded in finite time (Figure 5, curve E).

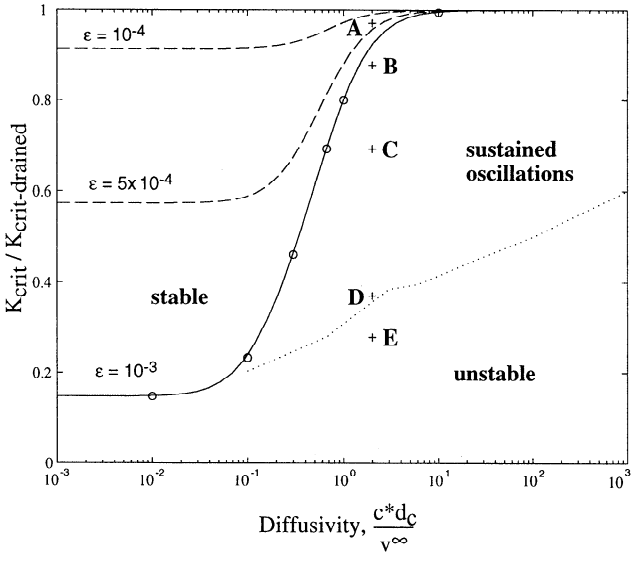

Figure 4. Critical spring stiffness dependence on normalized hydraulic diffusivity. Curves represent the analytical solution given by equation (24) for different values of ε. Open circles represent critical stiffness determined from numerical simulations for $\varepsilon = 1.0 \times 10^{-3}$. Letters refer to solutions shown in Figure 5. Dotted line approximately locates the boundary between limit cycles and unstable solutions, in the sense of approaching infinite velocity, for $\varepsilon = 1.0 \times 10^{-3}$. Other parameters are $b - a = 0.005$, $d_c = 10$ mm, $\sigma - p = 150$ MPa, $\beta = 1.0 \times 10^{-3}$ MPa^{-1}, and $\mu_{ss} = 0.64$.

Figure 4 illustrates the three types of possible behavior: a field of damped oscillations, a field of unstable slip, and an intervening field of finite amplitude oscillations. For sufficiently low diffusivities ($c^* d_c/v^\infty < 0.1$) the deformation is essentially undrained and finite amplitude oscillations can not exist for the one state variable friction law employed here. Interestingly, finite amplitude stick-slip like oscillations can exist even for $c^* d_c/v^\infty > 10$, conditions that would appear nominally drained. The reason for this is that fluid flow into the fault zone can not keep up with dilatancy at the high slip speeds obtained in these cases. Including inertia we would find that at sufficiently high diffusivity the finite oscillations would give way to dynamic stick-slip cycles.

Implications

In the limit of low hydraulic diffusivity, $c^* \to 0$, $\lambda \to 0$, and the function $F(c^*) \to 1$. In the undrained limit the critical stiffness is thus given by

$$k_{\text{crit-undrained}} = \frac{1}{d_c}\left[(\sigma - p)(b-a) - \frac{\varepsilon\mu_{ss}}{\beta}\right]. \qquad (27)$$

Since the critical stiffness must be nonnegative for unstable slip to occur, equation (27) places strong limits on the conditions under which fault slip instabilities can nucleate under undrained conditions. For example, if we take $(\sigma - p) = 180$ MPa (lithostatic minus hydrostatic load at 10 km); $b - a = 0.0025$ [*Kilgore et al.*, 1993], $\mu_{ss} = 0.64$, and $\beta = 5 \times 10^{-4}$ MPa^{-1} (see below), then $\varepsilon < 3.5 \times 10^{-4}$ for unstable slip to occur. Interestingly, the critical dilatancy coefficient is twice that estimated from *Marone et al.'s* [1990] experimental data. If ε from such data is appropriate for crustal faulting, then instabilities can occur under undrained conditions. If ε exceeds this critical value, then instability will be suppressed. It may be that this occurs at

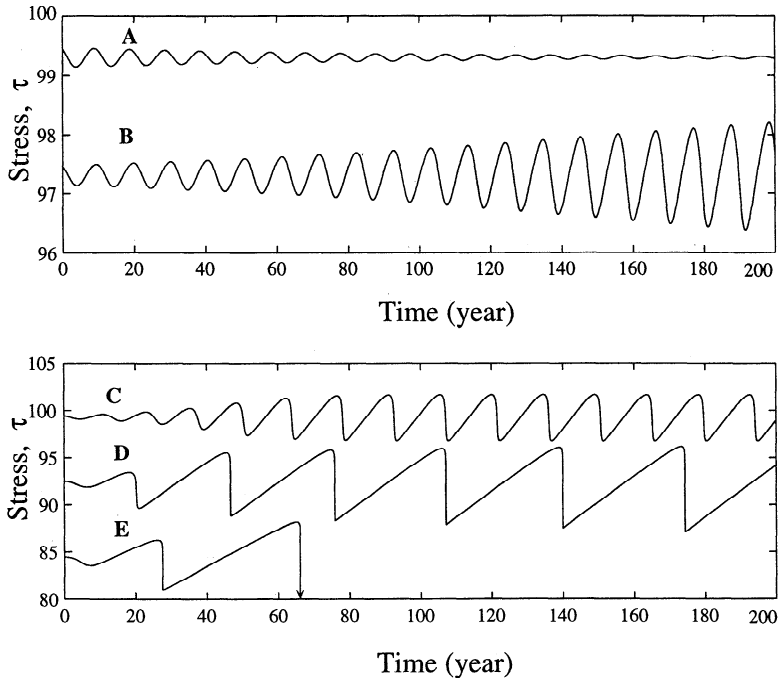

Figure 5. Numerical solutions showing the response to a small perturbation in velocity for different values of $k/k_{\rm crit}$. τ is in units of megapascals; the curves have been offset vertically for clarity. Letters are keyed to the points in Figure 4. Curve A, $k/k_{\rm crit} = 1.05$; curve B, $k/k_{\rm crit} = 0.95$; curve C, $k/k_{\rm crit} = 0.75$; curve D, $k/k_{\rm crit} = 0.4$; curve E, $k/k_{\rm crit} = 0.3$. Solutions B, C, and D approach a limit cycle. Solution E is unstable. The diffusivity is $c^* d_c/v^\infty = 2.0$, and the other parameters are as specified in Figure 4.

shallow depth on some faults and thus promotes stable afterslip in some earthquakes.

To estimate $\beta = \phi(\beta_f + \beta_\phi)$, we choose $\beta_f \sim 5 \times 10^{-4}$ MPa^{-1} and $\phi = 0.05$. This value of ϕ is at the lower end of the observed range for well-sheared Ottawa sand gouge in the laboratory for effective stresses up to 150 MPa [*Marone et al.*, 1990], but we use it because solution transport and mineralization processes at seismogenic depths may lead to greater densification. $\beta_\phi [\equiv \phi^{-1} \partial\phi/\partial p]$ is estimated from data of *David et al.* [1994], as the ratio of two parameters they call γ and α. They show in their Figure 7 that $\beta_\phi \sim 1 \times 10^{-2}$ MPa^{-1} for crystalline rocks and tight sandstones containing crack-like porosity, and $\beta_\phi \sim 1 \times 10^{-3}$ MPa^{-1} for porous sandstones. We expect the former to be more representative of fault gouge at seismogenic depths and take $\beta_\phi \sim 1 \times 10^{-2}$ MPa^{-1} and $\phi = 0.05$ which yields $\beta = 5 \times 10^{-4}$ MPa^{-1}.

Note also that for a given value of ε, and other constitutive parameters, pore pressure must be less than a critical value for instability to occur at all, that is for a sufficiently reduced k. Using (27), we find

$$\frac{p}{\sigma} < 1 - \frac{\varepsilon\mu}{\sigma\beta(b-a)}. \qquad (28)$$

Assuming values given above appropriate for 10 km depth, then the bounds on p/σ are as given in Figure 6. For example, assuming $b - a = 0.0025$ and ε estimated from the *Marone et al.'s* [1990] data, the ratio of pore pressure to normal stress must be less than 0.69 for instabilities to nucleate under undrained conditions. For ε greater than 5.5×10^{-4} the system is linearly stable for all $p/\sigma > 0$. Stated differently, equation (27) implies that $\varepsilon\mu_{ss}/\beta(b-a)$ is the smallest value of $(\sigma - p)$

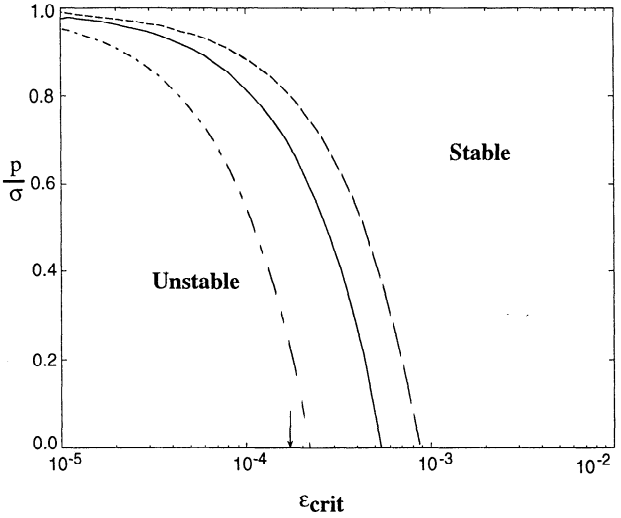

Figure 6. Limits on effective stress for slip instabilities to nucleate in the absence of pore fluid flow. See equation (28). Values of parameters are $\mu_{ss} = 0.64$, $\sigma = 280$ MPa, $\beta = 5.0 \times 10^{-4}$ MPa^{-1}. $b - a = 0.0025$ (solid curve), $b - a = 0.001$ (dash dotted curve), $b - a = 0.004$ (dashed curve). Arrow marks the value of ε estimated from the data of *Marone et al.* [1990].

for which instabilities can occur under undrained conditions. For the aforementioned parameters, $\sigma - p > 87$ MPa for undrained instability to be possible. This corresponds to the difference between overburden and hydrostatic pore pressure at about 4.8 km, a depth above which earthquake nucleation is rare. This is also in the depth range of stable after slip, although this may also result from a change in sign to $b - a < 0$ at low effective stress or in unconsolidated sedimentary cover, as suggested by *Marone et al.* [1991]. If ε appropriate for crustal faults is less than that for Ottawa sand, the depth is correspondingly shallower.

Note that numerous workers have called for high pore pressures to explain the apparent low frictional strength of the on the San Andreas, including the lack of a measurable heat flow anomaly. It was noted by *Lachenbruch* [1980] that hydraulic fracturing limits pore pressures to the least principal stress. *Rice* [1992] more recently pointed out that the pore pressure within a mature fault zone can exceed the least principal stress in the crust outside the fault. It is worth noting that stability considerations (equation (28)) also place limits on the magnitude of the pore pressure in regions where earthquake slip can nucleate without fluid exchange with the surroundings. Once dynamic slip is initiated it is possible for ruptures to propagate into regions where the effective stress is low. Low effective stress (high fault zone pore pressure) remains a viable explanation for the general behavior of the central creeping zone of the San Andreas, although some process must allow nucleation of small earthquakes there.

Simulations

We can describe the system behavior in a set of coupled first-order differential equations. We simulate inertial effects using a radiation damping term [*Rice*, 1993], so that the equation of motion becomes

$$k(v^{\infty}t - u) - (\sigma - p)\mu(v,\theta) = \eta v \qquad (29)$$

where $\eta = G/2v_s$, G is the shear modulus and v_s is the shear wave velocity [*Rice*, 1993]. This radiation damping term is an alternative to use of mdv/dt. The latter is correct for a lumped mass, but neither is fully suitable to simulate faulting in a continuum; the former predicts no dynamic overshoot, but the latter greatly overpredicts overshoot. In the simulations we sometimes employ a larger value of η for computational efficiency.

Differentiating (29) with respect to time leads to

$$\dot{v} = \left(\frac{\eta}{\sigma - p} + \frac{a}{v}\right)^{-1}\left[\frac{\dot{\tau} + \mu\dot{p}}{\sigma - p} - \frac{b\dot{\theta}}{\theta}\right] \qquad (30)$$

where $\dot{\tau}$ is given by (5) and $\dot{\theta}$ by (2). Note that positive stressing rate and increasing pore pressure cause the fault to accelerate, as does decreasing contact time (negative $\dot{\theta}$). In addition to these equations we include the state evolution equation (2), the elasticity equation (5), porosity evolution (14), and the diffusion equation (13). We thus have the following system of equations in the variables θ, τ, v, ϕ, and p

$$\frac{d\theta}{dt} = \dot{\theta}(\theta, v) \qquad (31a)$$

$$\frac{d\tau}{dt} = \dot{\tau}(v) \qquad (31b)$$

$$\frac{d\phi}{dt} = \dot{\phi}(\phi, v) \qquad (31c)$$

$$\frac{dp}{dt} = \dot{p}(p, \phi, v) \qquad (31d)$$

$$\frac{dv}{dt} = \dot{v}(p, \phi, v, \theta). \qquad (31e)$$

These coupled equations are solved using *Gear's* [1971] algorithm for stiff systems within MATLAB.

Figures 7, 8, 9, and 10 illustrate simulations in which the only parameter that varies is the hydraulic diffusivity c^*, which is expressed in units of reciprocal years. Parameter values are given in the captions; recall that slip and stress response depends on β and ε only through ε/β. The parameters are specified such that $k/k_{\text{crit-drained}} = 0.1$, but $k/k_{\text{crit-undrained}} = 62.5$; that is the system is unstable to drained deformation but stable to undrained deformation.

With infinite diffusivity ($c^* = 10^8$ years^{-1}), the deformation is drained and repeating stick slip events with a repeat time of roughly 80 years (Figure 7). With a diffusivity of ($c^* = 10$ yr^{-1}) there are stick slip events; however, the stress drops are considerably smaller and consequently the repeat time is reduced to roughly 30 years (Figure 8). Notice that the pore pressure drops by nearly 15 MPa, which transiently strengthens the fault, however for this diffusivity the pore pressure rapidly recovers. With a diffusivity of $c^* = 0.1$ yr^{-1} the dilatancy strengthening effect is further enhanced and the recurrence time is decreased to approximately 15 years (Figure 9). Notice that following the "initial event" the pore-pressure never significantly exceeds the far-field value of 100 MPa. Finally, when the diffusivity drops to $c^* = 0.01$ yr^{-1} (characteristic diffusion time of 100 years) the system becomes effectively undrained. Because of the choice of starting porosity, the fault initially undergoes a period of compaction. This causes the pore pressure to rise and triggers a stick slip event (Figure 10). However, following this initial event, the system evolves toward stable sliding, as predicted by the linearized stability analysis.

The transient dilatancy strengthening effect causes the magnitude of the stress drop during the stick-slip event to depend on the hydraulic diffusivity. Because the coefficient of friction itself is coupled to pore pressure, through dependence of the latter on slip speed, it is not possible to separate the frictional resistance into a drained component and a time-varying effective stress as is the case for slip-weakening friction [*Rudnicki and Chen*, 1988]. To see this, write the normalized shear resistance to slip as

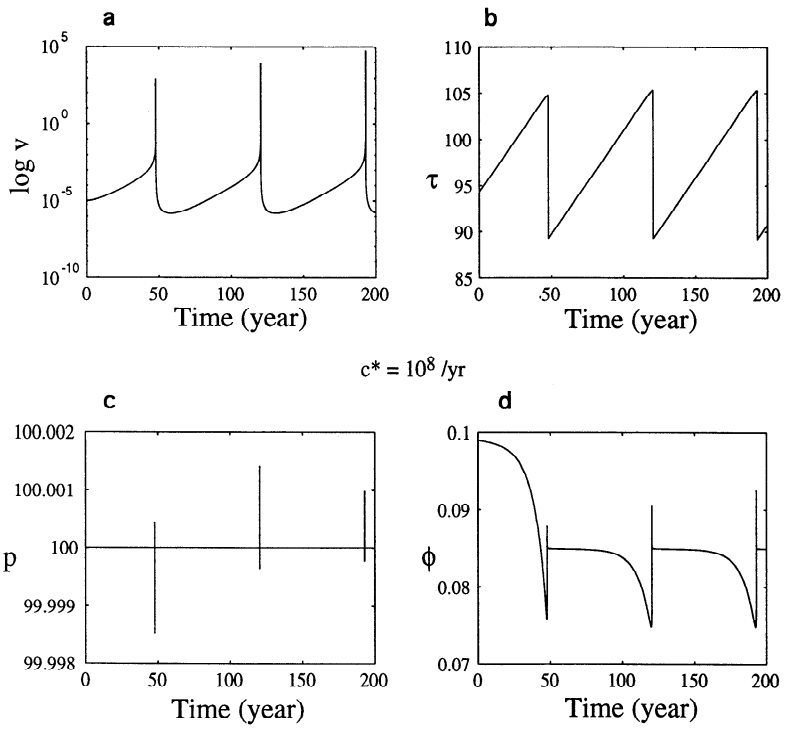

Figure 7. Simulation of stick slip cycle for drained conditions ($c^* = 10^8$ yr^{-1}). (a) Slip speed (m/yr) versus time. (b) Fault stress (MPa) versus time. (c) Pore pressure (MPa) versus time. (d) Porosity versus time. $k/k_{\text{crit-drained}} = 0.1$, $k/k_{\text{crit-undrained}} = 62.5$. $\mu_{ss} = 0.64$, $\sigma - p^\infty = 150$ MPa, $p^\infty = 100$ MPa, $\varepsilon = 1.17 \times 10^{-3}$, $\beta = 1.0 \times 10^{-3}$ MPa^{-1}. $b - a = 0.005$, $d_c = 0.01$ m, and $v^\infty = 0.03$ m/yr.

$$\frac{\tau(t)}{\sigma - p^\infty} = \frac{\sigma - p(t)}{\sigma - p^\infty}\mu(t). \tag{32}$$

In Figure 11a we see that the effective normal stress increases by ~ 10 % during a stick slip event. The friction coefficient μ decreases by a slightly greater amount (Figure 11b). The product of the two yields the normalized shear stress variation (32), which is shown in Figure 11c. Notice that the normalized stress drop is only a few percent, which is much less than the drop in μ. Furthermore, both the drop in frictional resistance and the drop in the coefficient of friction are less than the drop in friction under drained loading conditions (Figure 11d).

Dilatancy strengthening can have some interesting consequences, including one or more repeated slip events or "aftershocks" (Figure 12). In this case the diffusivity is sufficiently high that the pore pressure recovers soon after the "main shock," initiating a second stress drop event. It is noteworthy that these "aftershocks" are caused by rerupturing the same surface rather stress transfer to an adjoining part of the fault. Altering the diffusivity changes the magnitude of the dilatancy hardening effect and the timescale for the pore pressure transient to decay. Increasing the diffusivity diminishes the time to the aftershock as well as the stress drop in the aftershock. In some cases, multiple aftershocks occur (Figure 12). For very low diffusivities the time for the pressure transient to decay is too long and no aftershock occurs. For large diffusivities there is no dilatant hardening and thus no residual stress left to drive an aftershock.

Discussion

The simulations conducted here do not exhibit large transient pore pressure increases between earthquakes as could be attributed to the creep compaction mechanism discussed by *Sleep and Blanpied* [1992]. Rather, we observed pore pressure drops associated with the stick-slip events followed by recovery to values near to, or slightly greater than, the far-field pressure. If the initial porosity is greater than the equilibrium value, an initial period of compaction may raise the pore pressure significantly over the far-field pressure, triggering an unstable slip event (e.g., Figure 9). However, this is limited to the first stick-slip event and is not repeated after the system stabilizes.

While we are confident that the model presented here represents laboratory results for smooth gouge-filled faults with small displacements between instabilities, there are a number of effects that may occur in natural faults that are not accounted for. The constitutive relations employed here do not explicitly include viscous pore compaction as modeled by *Sleep and Blanpied* [1992]. Nor do we explicitly consider chemical cementation of faults between instabilities [*Fredrich and Evans*, 1992; *Blanpied et al.*, 1992]. Simulations using the alternate constitutive law for porosity (17), which does allow for (nonlinear) pore compaction under stationary contact, are qualitatively similar to those pre-

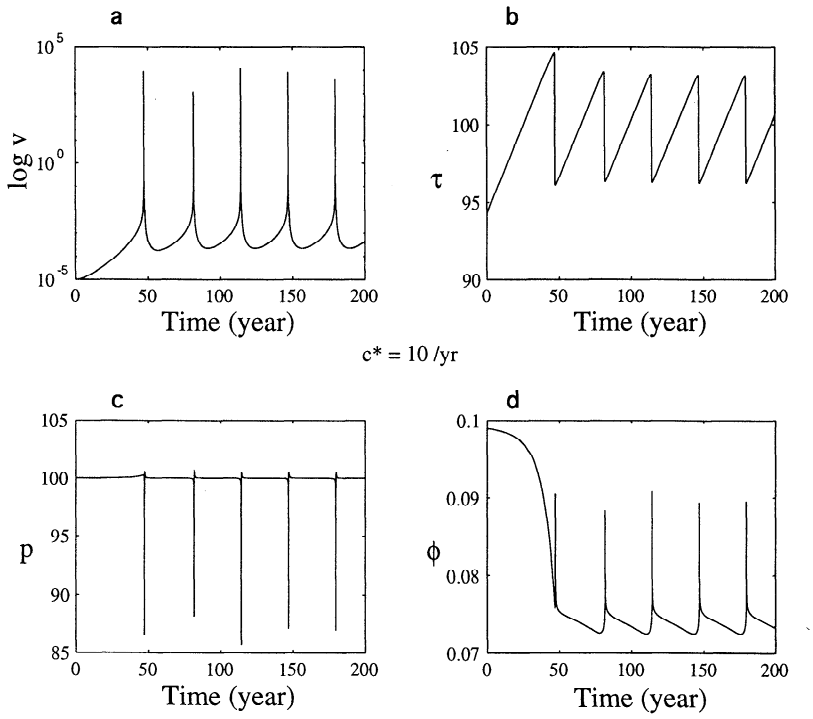

Figure 8. Simulation of stick slip cycle for hydraulic diffusivity $c^* = 10.0\ \mathrm{yr}^{-1}$. (a) Slip speed versus time. (b) Fault stress versus time. (c) Pore pressure versus time. (d) Porosity versus time. Other parameters are as given in Figure 7.

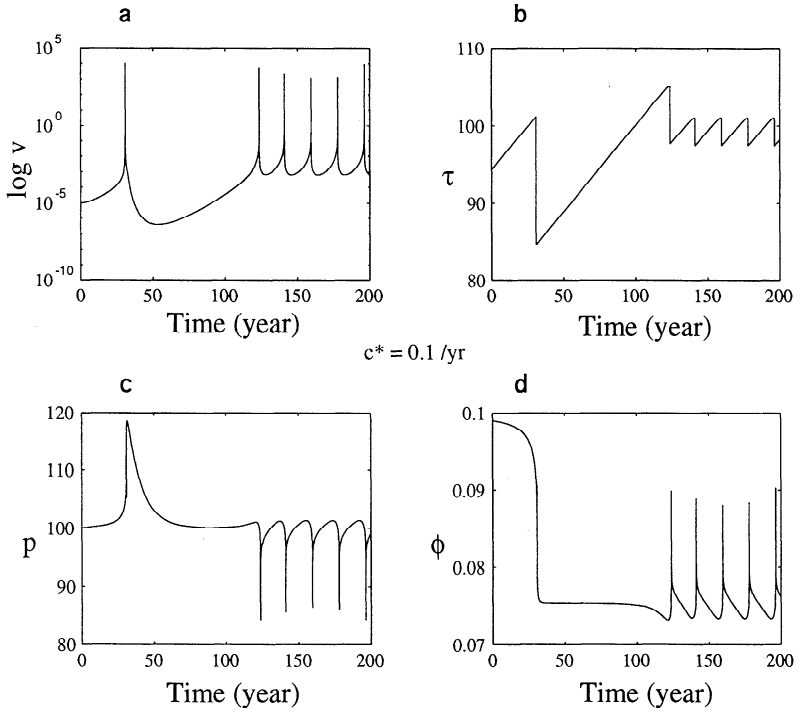

Figure 9. Simulation of stick slip cycle for hydraulic diffusivity $c^* = 0.1\ \mathrm{yr}^{-1}$. (a) Slip speed versus time. (b) Fault stress versus time. (c) Pore pressure versus time. (d) Porosity versus time. Other parameters are as given in Figure 7.

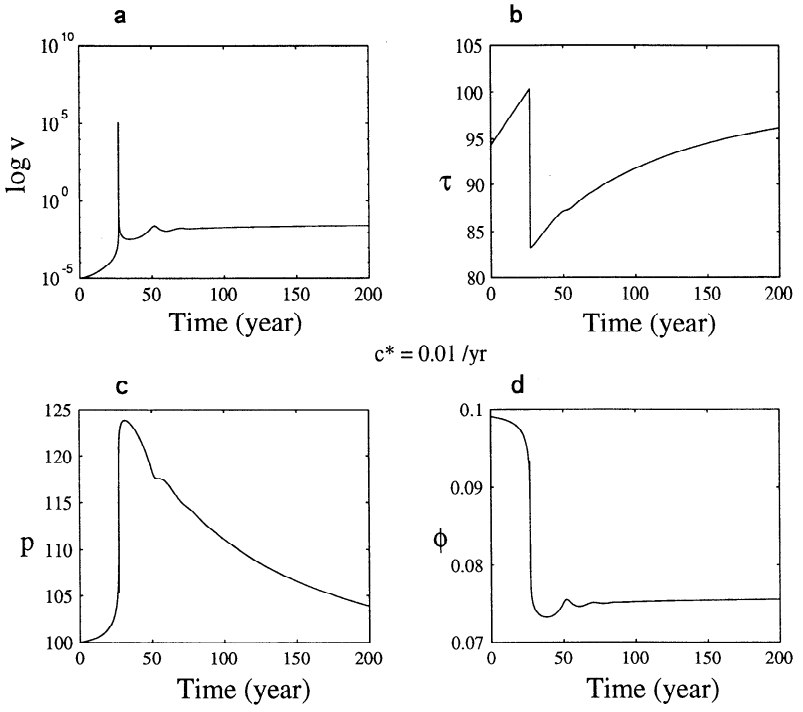

Figure 10. Simulation of stick slip cycle for hydraulic diffusivity $c^* = 0.01\ \mathrm{yr}^{-1}$. (a) Slip speed versus time. (b) Fault stress versus time. (c) Pore pressure versus time. (d) Porosity versus time. Other parameters are as given in Figure 7.

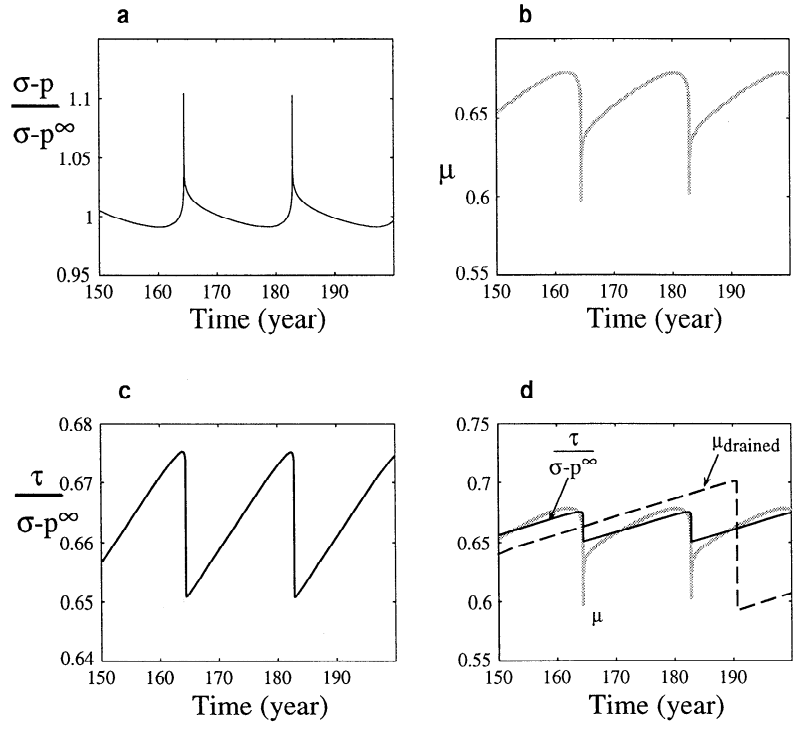

Figure 11. Dilatancy strengthening. (a) Effective stress $(\sigma - p(t))/(\sigma - p^{\infty})$; (b) coefficient of friction $\mu(t)$; (c) normalized frictional resistance $\tau(t)/(\sigma - p^{\infty})$; (d) comparison of normalized frictional resistance and $\mu(t)$ on the same scale. Note that dilatancy strengthening causes the normalized shear stress drop to be much less than the drop in the coefficient of friction. The drained behavior is shown for comparison.

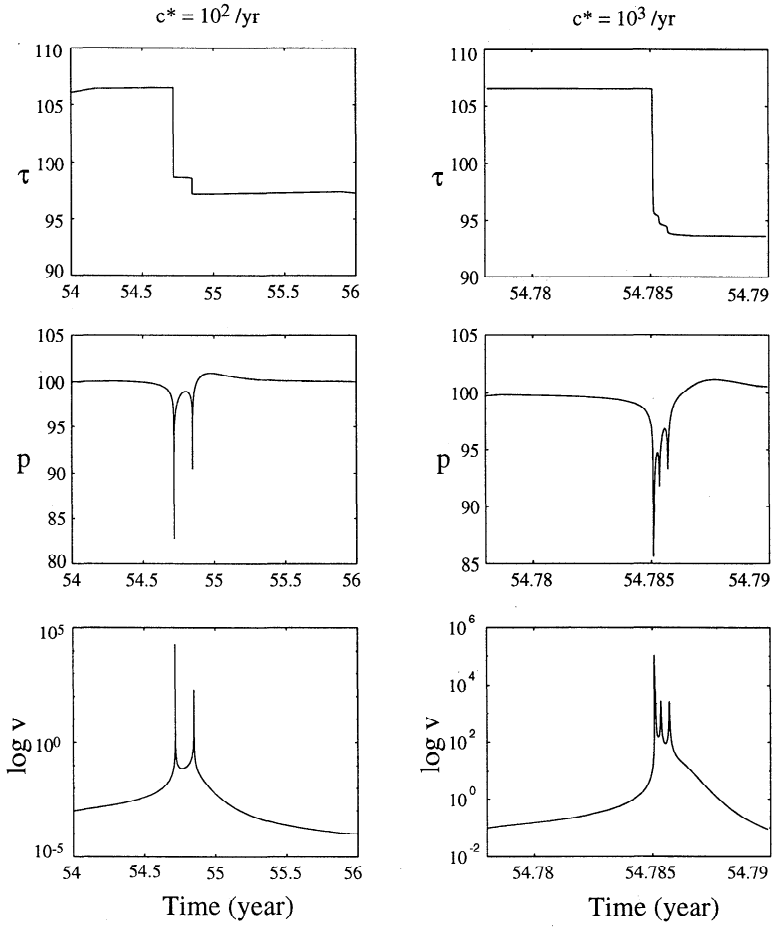

Figure 12. An example of model aftershocks induced by dilatancy strengthening. Dilatancy strengthening limits the stress drop in the "mainshock". Rapid diffusion into the fault restores the pore pressure and induces an "aftershock". $d_c = 0.001$ m, $k/k_{\text{crit-drained}} = 0.01$, $k/k_{\text{crit}_u\text{ndrained}} = 6.25$. Other parameters are as given in Figure 7. (left) The stress, pore pressure, and slip speed for $c^* = 10^2$ yr^{-1}. (right) The effect of increasing the hydraulic diffusivity c^* by a factor of 10. Notice that the time axis is expanded to show the events clearly.

sented here. Inclusion of linear viscous pore compaction is unlikely to alter our principal conclusions concerning stability of fault slip. Viscous pore compaction could slightly counter the effects of dilatancy, but only if the characteristic time for pore compaction $\beta\nu$, where ν is viscosity, is comparable to the characteristic time for state evolution d_c/v^∞. The latter is of the order of 1 year or less, for $d_c \leq 1$ cm. Large-scale pore compaction during the interseismic period has the effect of raising pore pressure and promoting stable sliding.

An alternate formulation for dilatancy , examined by *Marone et al.* [1990] and N. Beeler and T.E. Tullis (unpublished manuscript, 1995), derives from an old, but imprecise notion in soil mechanics that in the presence of dilation the effective friction coefficient is augmented by the ratio of normal strain rate to shear strain rate [e.g., *Schofield and Wroth*, 1968]. These strain rates are $\dot{\phi}/(1-\phi)$ and v/h, respectively, where h is the thickness of the fault zone, so that

$$\mu = \mu_1(v,\theta) + \frac{h\dot{\phi}}{v(1-\phi)} \tag{33}$$

where μ_1 is some hypothetical coefficient of friction in the absence of dilatancy, that is described in the form of (1) but in which we replace a and b with a_1 and b_1. It is interesting to note that when combined with the first formulation for ϕ and $\dot{\phi}$, equations (14) and (15), when there is a sudden change in velocity from say v_0 at steady state to a new value v, the term $h\dot{\phi}/v(1-\phi)$ changes suddenly by $[h\varepsilon/d_c(1-\phi_0)]\ln(v/v_0)$ and then decays toward zero with ongoing slip. This is qualitatively similar to the basic friction effect described by equations (1) and (2) with $a = b = h\varepsilon/d_c(1-\phi_0)$, so that some aspect of the direct and evolutionary response may be related to dilatancy. Nevertheless, the relation is not simple, and does not explain steady state changes in friction. Furthermore, for gouge, *Marone et al.* [1990] and N. Beeler and T.E. Tullis (unpublished manuscript, 1995) suggest that $h\varepsilon/d_c(1-\phi_0)$ overestimates a by several times, whereas the latter workers find that a is reasonably estimated for bare granite surfaces. Note that $h\dot{\phi}/(1-\phi)$ is just the opening rate across the fault layer. With this friction law (33) we have the remarkable result that for linear perturbations about steady

state, it yields identical predictions to the one based on equations (1), (2), (14), and (15), so long as we identify $a = a_1 + h\varepsilon/d_c(1-\phi_0)$ and $b = b_1 + h\varepsilon/d_c(1-\phi_0)$.

Earthquakes for which coseismic slip at depth exceeds the slip at the Earth's surface often exhibit stable afterslip. Decelerating creep following the 1966 Parkfield earthquake is one example of this phenomenon. *Marone et al.* [1991] propose that earthquake afterslip results from inherent velocity strengthening behavior ($a - b > 0$) of shallow fault zone materials. To this we add the possibility that shallow fault zone materials may tend to be more dilatant, due to low lithostatic stress at these depths, than the fault zone at seismogenic depths. The shallow fault zone response to rapid, undrained, coseismic loading may be stabilizing if the dilatancy coefficient is sufficiently large (see equation (27)).

Up to this point we have assumed that changes in pore pressure alter the frictional resistance only through the effective stress. That is, we have assumed that changes in pore-pressure have no effect on the coefficient of friction, μ. *Linker and Dieterich* [1992] show that step increases in normal stress at fixed load-point velocity cause transient decreases in μ, followed by an evolution back to steady state. They interpret this as due to a normal stress effect on state and suggest evolution laws of the form

$$\frac{d\theta}{dt} = 1 - \frac{\theta v}{d_c} - \frac{\alpha\theta(\dot{\sigma} - \dot{p})}{b(\sigma - p)} \tag{34}$$

[*Dieterich and Linker*, 1992; equation (5)], where α is an experimentally derived constant which takes on values $0.2 < \alpha < 0.5$. While this effect has yet to be demonstrated for gouge-filled faults, the Linker-Dieterich normal stress effect can be expected to slightly increase the critical spring stiffness as computed by (24). Dilatancy-induced increases in effective stress cause a transient decrease in state and thus in friction coefficient. This weakening effect slightly, but never completely, counteracts the effect of dilatancy strengthening, as illustrated in Figure 13. This shows that for given ε, $k_{\text{crit-undrained}}$ does not vary significantly over the allowable range of α, $0 < \alpha < 0.5$. An expression for the critical stiffness under undrained loading ($c^* = 0$) including the Linker-Dieterich effect is given in Appendix B.

Finally, it is clear that we do not accurately model all processes active at high slip speeds. We have not, for example, considered the effects of a high-speed "cut-off" in the steady state weakening, nor the possibility of undulations in normal stress from rapid sliding on a rough surface. Furthermore, we have not considered the effects of shear heating and thermal pressurization of pore fluids. High-speed phenomena will not alter the stability analysis which considers perturbations about steady state. However, these phenomena could have a profound effect on the simulations of the earthquake cycle. In particular, dilatancy strengthening effects may be completely negated at large slip by shear heating induced thermal pressurization. This could considerably alter the simulations exhibiting aftershock like behavior. A more fundamental problem (which we leave to a following paper, but have partially discussed elsewhere [*Rice*, 1994; *Segall and Rice*, 1995]) is to determine under what conditions shear heating is capable of nucleating unstable slip in the absence of steady state velocity weakening. Our considerations thus far suggest that if d_c is in the range of laboratory values, and thus considerably less than the characteristic slip distance associated with shear heating, unstable friction as discussed here will nucleate instabilities. Following the onset of unstable slip, shear heating comes into play and may control behavior for large slip magnitude.

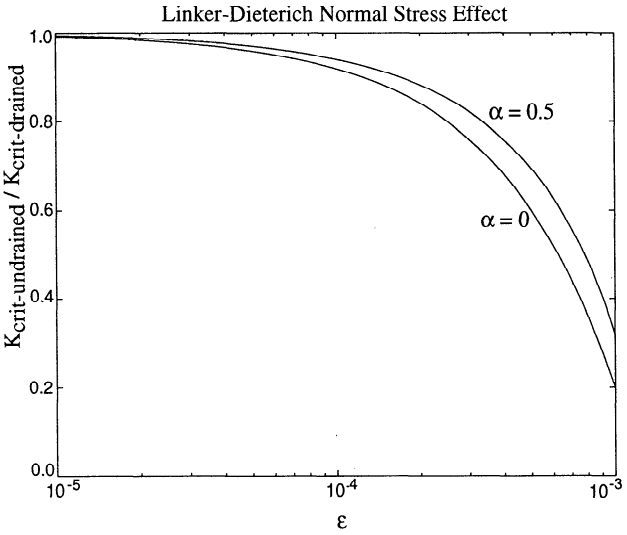

Figure 13. Influence of Linker-Dieterich normal stress effect on critical stiffness for undrained loading. Undrained critical stiffness normalized by drained value is plotted as a function of dilatancy coefficient ε for $\alpha = 0$ and $\alpha = 0.5$. Other parameters are $b - a = 0.005$, $d_c = 10$ mm, $\sigma - p = 150$ MPa, $\beta = 1.0 \times 10^{-3}$ MPa^{-1}, and $\mu_{ss} = 0.6$

There is evidence for aftershocks occurring within mainshock slip zones. While aftershocks tend to be concentrated around areas of high mainshock slip [*Menodza and Hartzell*, 1988; *Beroza and Spudich*, 1988], there are usually some aftershocks located within these zones. For example, in the 1989 Loma Prieta earthquake, right-lateral aftershocks are found within the zone of high mainshock slip southeast of the hypocenter determined from the inversion of strong motion [e.g., *Beroza*, 1991; *Steidl et al.*, 1991; *Wald et al.*, 1991] and geodetic [*Arnadottir and Segall*, 1994] data. *Beroza and Zoback* [1993] found that 20% (191 of 979 events studied) of the Loma Prieta aftershocks fall into the category of "delayed mainshock rupture" (G. Beroza, written communication, 1995); that is, events for which the mainshock reduces the shear traction and for which the change in shear traction and aftershock slip vector act in opposite directions. It is, of course, possible that the slip inversions are inaccurate, although the general similarity between inversions based on geodetic and strong motion data suggests the overall slip pattern is signifi-

cant. It is also possible that these aftershocks occur in slip deficient zones that are too small to be resolved by either data set. Nevertheless, the best available data do suggest that aftershocks do occur in regions of significant coseismic slip. Such events, if they occur, are not easily explained by conventional models of aftershocks. *Dieterich's* [1994] analysis based on drained rate and state dependent friction explains Omori's law, assuming that aftershock nucleation sites experience a static increase in shear stress (or decrease in normal stress) at the time of the mainshock. His specific calculations are restricted to fault segments that were unruptured in the mainshock. *Nur and Booker* [1972] discussed a model for inducing aftershocks off the mainshock rupture plane, by pore fluid flow, but again do not address aftershocks within the mainshock slip zone. With the caveats of the previous paragraph in mind, we suggest that aftershocks within the mainshock rupture might occur by a combination of mainshock dilatancy and subsequent rapid repressurization of fault zone fluids.

Conclusions

Dilatancy of a fluid-saturated fault favors, but does not require, stable sliding. Whether slip is unstable or not depends on the relative magnitude of frictional (steady state velocity) weakening and dilatancy strengthening. Creeping zones along faults, as well as the tendency for shallow afterslip following moderate-sized earthquakes, may reflect dilatant fault zone materials, low effective stresses, and/or steady state velocity strengthening behavior. If ambient pore pressures exceed some fraction of the fault normal stress, or if effective stress is low enough, earthquakes cannot nucleate under undrained conditions. Thus, while near lithostatic fault zone pore pressure may resolve the "weak fault" problem, extreme pore pressures may at the same time prohibit earthquakes from nucleating without fluid exchange with the surroundings. If pressurized fault zones are effectively isolated from adjoining crust, then extremely high fault zone pore pressure may be a better explanation for the central creeping zone of the San Andreas fault than for the presently locked zones that experience large earthquakes.

Our simulations with rate- and state-dependent friction and dilatancy exhibit complex behavior, including rerupturing of the same fault surface due to dilatancy strengthening during rapid slip followed by fluid flow and recovery of pore pressure is observed under some conditions. This may explain the apparent occurrence of aftershocks within zones of substantial mainshock slip. In general, many aspects of the system behavior, including stress drop and recurrence time, depend on characteristic time for fluid diffusion.

Appendix A: Stability Analysis

Substituting exponential forms $\Delta p = Pe^{st}$, $\Delta\theta = \Theta e^{st}$, $\Delta v = Ve^{st}$, $\Delta\phi = \Phi e^{st}$ into the linearized equations (23) yields a cubic equation in s,

$$(\sigma - p)as = (\sigma - p)b\frac{rs}{r+s} - \frac{\mu_{ss}\varepsilon}{\beta}\frac{rs^2}{(c^* + s)(r+s)} - krd_c \tag{A1}$$

where $r = v^\infty/d_c$. The roots of (A1), s_j, determine the critical stiffness. First, note that in the limit that kd_c becomes infinite, that $\Re(s_j) < 0$ for $j = 1, 2, 3$, so that all perturbations from steady state are damped in finite time. The critical stiffness is determined by the largest value of kd_c for which $\Re(s_j) > 0$ for some j. Since no root $s = 0$ exists with nonzero k, we assume that the first root to cross to the real half plane does so at $s = i\rho$. Thus, (A1) becomes

$$\begin{aligned} i(\sigma - p)a\rho = \\ i(\sigma - p)b\frac{r\rho}{r + i\rho} + \frac{\mu_{ss}\varepsilon}{\beta}\frac{r\rho^2}{(c^* + i\rho)(r + i\rho)} \\ - r\, k_{\text{crit}}\, d_c. \end{aligned} \tag{A2}$$

Equating the real and imaginary parts of (A2),

$$\begin{aligned} 0 = \\ (\sigma - p)b\frac{r\rho^2}{r^2 + \rho^2} + \frac{\mu_{ss}\varepsilon}{\beta}\frac{r\rho^2(rc^* - \rho^2)}{(r^2 + \rho^2)[(c^*)^2 + \rho^2]} \\ - r\, k_{\text{crit}}\, d_c \end{aligned} \tag{A3a}$$

$$\begin{aligned} (\sigma - p)a\rho = \\ (\sigma - p)b\frac{r^2\rho}{r^2 + \rho^2} - \frac{\mu_{ss}\varepsilon}{\beta}\frac{r\rho^3(c^* + r)}{(r^2 + \rho^2)[(c^*)^2 + \rho^2]}. \end{aligned} \tag{A3b}$$

Equations (A3a) and (A3b) give the solution for ρ, the frequency of oscillation at neutral stability, and k_{crit}. Equation (A3a) can be put in a simpler form by dividing the first by r and the second by ρ and then adding

$$k_{\text{crit}}d_c = (\sigma - p)(b - a) - \frac{\mu_{ss}\varepsilon}{\beta}\frac{\rho^2}{(c^*)^2 + \rho^2}. \tag{A4}$$

In the undrained limit $c^* = 0$ this yields the result in the text; ρ^2 is determined by (A3b). To do so, we introduce the variable

$$z = \frac{\rho^2}{(c^*)^2 + \rho^2}. \tag{A5}$$

Introducing z into (A3b) yields a quadratic equation in z

$$z^2 - (1 + \lambda + \gamma)z + \gamma = 0, \tag{A6}$$

where

$$\lambda = \frac{\beta(\sigma - p)a(c^*)^2}{\mu_{ss}\varepsilon r(c^* + r)} \tag{A7a}$$

$$\gamma = \frac{\beta(\sigma - p)(b - a)r}{\mu_{ss}\varepsilon(c^* + r)}. \tag{A7b}$$

Note that $\lambda > 0$ as long as the effective stress is compressive, and that $\gamma > 0$ if the system can exhibit unstable slip under drained conditions ($b-a > 0$). Thus solutions are

$$z = \frac{1+\lambda+\gamma}{2} \pm \sqrt{\frac{(1+\lambda+\gamma)^2}{4} - \gamma}. \qquad \text{(A8)}$$

It can be shown that term under the radical is always positive and thus z is always real. Because k_{crit} decreases with increasing z the relevant root is the smallest. Thus the critical stiffness is given by (24) of the text.

Appendix B: Normal Stress Effect on Critical Stiffness

In replacing (23b) with the linearized form of the evolution law (34), we assume that the applied normal stress is held constant, leading to

$$\Delta\dot{\theta} = -\frac{v^\infty}{d_c}\Delta\theta - \frac{1}{v^\infty}\Delta v + \frac{\alpha d_c}{bv^\infty(\sigma-p)}\Delta\dot{p}. \qquad \text{(B9)}$$

Following the procedure outlined in Appendix A leads to an expression for the critical stiffness including the Linker-Dieterich normal stress effect on state. In order to keep the analysis tractable we restrict attention to the undrained limit $c^* = 0$. In this limit we find

$$k_{\text{crit-undrained}} = \frac{1}{d_c}\left\{(\sigma-p)(b-a) - \frac{\varepsilon\mu_{ss}}{\beta} + \frac{\alpha\varepsilon}{\beta} \times \left[\frac{1-\zeta}{2} + \sqrt{\frac{(\zeta-1)^2}{4} + \chi}\right]\right\} \qquad \text{(B10)}$$

where

$$\zeta = \frac{\beta(\sigma-p)b}{2\alpha\varepsilon} - \frac{\mu_{ss}}{2\alpha} \qquad \text{(B11a)}$$

$$\chi = \frac{\beta(\sigma-p)(b-a)}{2\alpha\varepsilon} - \frac{\mu_{ss}}{2\alpha}. \qquad \text{(B11b)}$$

Acknowledgments. We thank Chris Marone for providing experimental data and David Lockner for preprints of papers with James Byerlee. This work was in large part stimulated by, and profited from, discussions with Norman Sleep, Michael Blanpied, and Nicholas Beeler which we gratefully acknowledge. P.S. would like to thank Andy Ruina and James Dieterich for long ago introducing him to the intricacies of friction, an interest which ultimately led to this publication. We thank Linda Reinen, Joanne Fredrich, Joseph Walder, and Teng Fong Wong for thoughtful comments, those of the latter also contributed to our understanding of pore compressibility. Yijun Du provided invaluable assistance with the figures. This research was in part supported by D.O.E. Office of Basic Energy Sciences grant DE-FG03-90ER14152 to Stanford, U.S. Geological Survey NEHRP grant 1434-93-G-2450 to Harvard, and an Allan Cox Visiting Professorship to J.R.R. at Stanford.

References

Arnadottir, T. and P. Segall, The 1989 Loma Prieta earthquake imaged from the inversion of geodetic data, *J. Geophys. Res., 99,* 21,835–21,855, 1994.

Beroza, G. C., Near-source modeling of the Loma Prieta earthquake: Evidence for heterogeneous slip and implications for earthquake hazard, *Bull. Seismol. Soc. Am., 81,* 1603–1621, 1991.

Beroza, G. C., and P. Spudich, Linearized inversion for fault rupture behavior; application to the 1984 Morgan Hill, California, earthquake, *J. Geophys. Res., 93,* 6275-6296, 1988.

Beroza, G. C., and M. D. Zoback, Mechanism diversity of the Loma Prieta aftershocks and the mechanics of mainshock-aftershock interaction, *Science, 259,* 210-213, 1993.

Blanpied, M. L., D. A. Lockner, and J. D. Byerlee, Fault stability inferred from granite sliding experiments at hydrothermal conditions, *Geophys. Res. Lett., 18,* 609-612, 1991.

Blanpied, M. L., D. A. Lockner, and J. D. Byerlee, An earthquake mechanism based on rapid sealing of faults, *Nature, 358(6387),* 574-576, 1992.

Byerlee, J. D. , Friction, overpressure and fault normal compression, *Geophys. Res. Lett., 17,* 2109-2112, 1990.

Byerlee, J. D., Model for episodic flow of high-pressure water in fault zones before earthquakes, *Geology, 21,* 303-306, 1993.

David, C., T.-F. Wong, W. Zhu, and J. Zhang, Laboratory measurement of compaction-induced permeability change in porous rocks; implications for the generation and maintenance of pore pressure excess in the crust, *Pure Appl. Geophys., 143,* 425-456, 1994.

Dieterich, J. H., Time-dependent friction and the mechanics of stick-slip, *Pure Appl. Geophys., 116,* 790-806, 1978.

Dieterich, J. H., Modeling of rock friction, 1, Experimental results and constitutive equations, *J. Geophys. Res., 84,* 2161-2168, 1979.

Dieterich, J. H., A model for the nucleation of earthquake slip, *in Earthquake Source Mechanics, Geophys. Monogr. Ser.,* vol. 37, edited by S. Das, J. Boatwright, and C. H. Scholz, pp. 37-47, AGU, Washington, D.C., 1986.

Dieterich, J. H., Nucleation and triggering of earthquake slip; effect of periodic stresses, *Tectonophysics, 144,* 127-139, 1987.

Dieterich, J. H., Earthquake nucleation on faults with rate- and state-dependent strength, *Tectonophysics, 211,* 115-134, 1992.

Dieterich, J. H., A constitutive law for rate of earthquake production and its application to earthquake clustering, *J. Geophys. Res., 99,* 2601-2618, 1994.

Dieterich, J. H., and M. F. Linker, Fault stability under conditions of variable normal stress, *Geophys. Res. Lett., 19,* 1691-1694, 1992.

Fredrich, J., and B. Evans, Strength recovery along simulated faults by solution transfer processes, *Proc. 33rd U.S. Symp. Rock Mech.,* 121-130, 1992.

Gear, C.W., *Numerical Initial Value Problems in Ordinary Differential Equations,* Prentice-Hall, Englewood Cliffs, N. J., 1971.

Gu, J.-C., J.R. Rice, A.L. Ruina, and S.T. Tse, Slip motion and stability of a single degree of freedom elastic system with rate and state dependent friction, *J. Mech. Phys. Solids, 32*, 167-196, 1984.

Horowitz, F. G., and A. Ruina, Slip patterns in a spatially homogeneous fault model, *J. Geophys. Res., 94*, 10,279-10,298, 1989.

Kilgore, B. D., J. H. Dieterich, and M. L. Blanpied, Velocity dependent friction of granite over a wide range of conditions, *Geophys. Res. Lett., 20*, 903-906, 1993.

Lachenbruch, A. H., Frictional heating, fluid pressure, and the resistance to fault motion, *J. Geophys. Res., 85*, 6097-6112, 1980.

Lambe, T. W., and R. V. Whitman, *Soil Mechanics*, John Wiley, New York, 1969.

Linker, M. F., and J. H. Dieterich, Effects of variable normal stress on rock friction, observations and constitutive equations, *J. Geophys. Res., 97*, 4923-4940, 1992.

Lockner, D.A., and J.D. Byerlee, Dilatancy in hydraulically isolated fault and the suppression of instability, *Geophys. Res. Lett., 21*, 2353-2356, 1994.

Marone, C., and C. H. Scholz, The depth of seismic faulting and the upper transition from stable to unstable slip regimes, *Geophys. Res. Lett., 15*, 621-624, 1988.

Marone, C., C.B. Raleigh, and C.H. Scholz, Frictional behavior and constitutive modeling of simulated fault gouge, *J. Geophys. Res., 95*, 7007-7025, 1990.

Marone, C., C.H. Scholz, and R. Bilham, On the mechanics of earthquake afterslip, *J. Geophys. Res., 96*, 8441-8452, 1991.

Mase, C. W., and L. Smith, Effects of frictional heating on the thermal, hydrologic, and mechanical response of a fault, *J. Geophys. Res., 92*, 6249-6272, 1987.

Menodza, C., and S. Hartzell, Aftershock patterns and main shock faulting, *Bull. Seismol. Soc. Am., 78*, 1438-1449, 1988.

Morrow, C, A., and J.D. Byerlee, Experimental studies of compaction and dilatancy during frictional sliding on faults containing gouge, *J. Struct. Geol., 11*, 815-825, 1989.

Nur, A., and J.R. Booker, Aftershocks caused by pore fluid flow?, *Science, 175(4024)*, 885-887, 1972.

Reinen, L. A., and J. D. Weeks, Determination of rock friction constitutive parameters using an iterative least squares inversion method, *J. Geophys. Res., 98* 15,937-15,950, 1993.

Rice, J. R, On the stability of dilatant hardening for saturated rock masses, *J. Geophys. Res., 80*, 1531-1536, 1975.

Rice, J. R., Fault stress states, pore pressure distributions, and the weakness of the San Andreas Fault, in *Fault Mechanics and Transport Properties of Rocks; A Festschrift in Honor of W. F. Brace*, edited by B. Evans, and T.-F. Wong, pp. 475-503, Academic Press, New York, 1992.

Rice, J. R., Spatio-temporal complexity of slip on a fault, *J. Geophys. Res., 98*, 9885-9907, 1993.

Rice, J. R., Earthquakes at low driving stress in a high strength, low toughness fault zone: Shear heating example (abstract), *Eos Trans. AGU, 75(44)*, Fall Meet. Suppl., 426, 1994.

Rice, J. R., and A. Ruina, Stability of steady frictional sliding, *J. Appl. Mech., 50*, 343-349, 1983.

Rice, J. R., and S. T. Tse, Dynamic motion of a single degree of freedom system following a rate and state dependent friction law, *J. Geophys. Res., 91*, 521-530, 1986.

Rudnicki, J. W., and C.-H. Chen, Stabilization of rapid frictional slip on a weakening fault by dilatant hardening, *J. Geophys. Res., 93*, 4745-4757, 1988.

Ruina, A., Slip instability and state variable friction laws, *J. Geophys. Res., 88*, 10,359-10,370, 1983.

Schofield, A. N., and C. P. Wroth, *Critical State Soil Mechanics*, McGraw-Hill, New York, 1968.

Segall, P. and J.R. Rice, Slip instabilities: Unstable friction or shear heating? (abstract), *IUGG XXI General Assembly Abstracts*, Boulder, Colo., A357, 1995.

Sibson, R. H., Interactions between temperature and pore-fluid pressure during earthquake faulting and a mechanism for partial or total stress relief, *Nature, 243(126)*, 66-68, 1973.

Sibson, R. H., Implications of fault-valve behaviour for rupture nucleation and recurrence, *Tectonophysics, 211*, 283-293, 1992.

Sibson, R. H., F. Robert, and K. H. Poulsen, High-angle reverse faults, fluid-pressure cycling, and mesothermal gold-quartz deposits, *Geology, 16*, 551-555, 1988.

Sleep, N. H., Ductile creep, compaction, and rate and state dependent friction within major fault zones, *J. Geophys. Res., 100*, 13,065-13,080, 1995.

Sleep, N. H., and M. Blanpied, Creep, compaction and the weak rheology of major faults, *Nature, 359(6397)*, 687-692, 1992.

Steidl, J. H., R. J. Archuleta, and S. H. Hartzell, Rupture history of the 1989 Loma Prieta, California, earthquake, *Bull. Seismol. Soc. Am., 81*, 1573–1602, 1991.

Stuart, W. D., Forecast model for great earthquakes at the Nankai Trough subduction zone, *Pure Appl. Geophys., 126*, 619-641, 1988.

Tse, S. T., and J.R. Rice, Crustal earthquake instability in relation to the depth variation of frictional slip properties, *J. Geophys. Res., 91*, 9452-9472, 1986.

Tullis, T. E., Rock friction constitutive behavior from laboratory experiments and its implications for an earthquake prediction field monitoring program, *Pure Appl. Geophys., 126*, 555-588, 1988.

Wald, D. J., D. V. Helmberger, and T. H. Heaton, Rupture model of the 1989 Loma Prieta earthquake from the inversion of strong-motion and broadband teleseismic data, *Bull. Seismol. Soc. Am., 81*, 1540–1572, 1991.

Walder, J., and A. Nur, Porosity reduction and crustal pore pressure development, *J. Geophys. Res., 89*, 11,539-11,548, 1984.

Zoback, M.D., and J.D. Byerlee, Effect of high-pressure deformation on permeability of Ottawa sand, *Am. Assoc. Pet. Geol. Bull., 60*, 1531-1542, 1976.

J. R. Rice, Department of Earth and Planetary Sciences, and Division of Applied Sciences, Harvard University, Cambridge, MA 02138. (e-mail: rice@esag.harvard.edu)

P. Segall, Department of Geophysics, Stanford University, Stanford, CA 94305. (e-mail: segall@pangea.stanford.edu)

(Received February 22, 1995; revised July 27, 1995; accepted August 4, 1995.)